Testing photo-reduction of gaseous oxidized mercury (Hg^{II})

A new mechanism of Hg^{II} photo-reduction in gaseous phase was recently suggested by *Saiz-Lopez et al.* [2018]. To investigate possibility and importance of the new mechanism the GLEMOS chemical transport model was applied for test simulations on a global scale. For the sake of the study the most recent form of the two-step Br oxidation mechanism was implemented in the GLEMOS model [*Ilyin et al.*, 2018; *Saiz-Lopez et al.,* 2018]. An experimental version the model considers six Hg chemical species in the atmosphere: Hg^0, unstable intermediate Hg^IBr and four Hg^{II} species ($HgBr_2$, HgBrOH, HgBrOOH, HgBrONO). The Hg^{II} species are simulated in both gaseous and particulate state using the parameterisation of gas-particle partitioning from [*Amos et al.*, 2012]. Details of the chemical mechanism implemented in the model as well as the reaction rate constants are given in Table 1. In addition to the oxidation reactions we also included gas-phase photo-reduction of $HgBr_2$, HgBrOH, HgBrOOH, HgBrONO using the photolysis rates calculated by the CAM-Chem model [*Saiz-Lopez et al.*, 2018]. Six-hourly concentration fields of Br were archived from a GEOS-Chem simulation [*Parrella et al.,* 2012], whereas OH, HO_2, NO_2 and particulate matter (PM2.5) fields were imported from MOZART [*Emmons et al.*, 2010].

Table 1. *Experimental chemical mechanism for atmospheric Hg in GLEMOS*

N	Reaction	Rate, molecule cm^{-3} s^{-1}	Reference
R1	$Hg^0 + Br + M \rightarrow Hg^IBr + M$	1.5×10^{-32} $(T/298)^{-1.86}$ $[Hg^0][Br][M]^{(a)}$	*Donohoue et al*. [2006]
R2	$Hg^IBr + M \rightarrow Hg^0 + Br + M$	1.6×10^{-9} exp(-7801/T) [HgBr][M]	*Dibble et al*. [2012]
R3	$Hg^IBr + Br \rightarrow Hg^0 + Br_2$	3.9×10^{-11} [HgBr][Br]	*Balabanov et al*. [2005]
R4	$Hg^IBr + Y \overset{M}{\rightarrow} Hg^{II}BrY$ *Y* = Br, OH, NO_2, HO_2	*Y = Br, OH* : 2.5×10^{-10} $(T/298)^{-0.57}$ [HgBr][Y] *Y = NO_2, HO_2* : k_Y ([M],T)[HgBr][Y]	*Goodsite et al*. [2004] *Jiao and Dibble* [2017]
R5	$Hg^{II}BrY \overset{h\nu}{\rightarrow} Hg^0 + products$ *Y* = Br, OH, NO_2, HO_2	k_{photo} [HgBrY]	*Saiz-Lopez et al*. [2018]
R6	$Hg^{II}BrY \overset{h\nu}{\rightarrow} Hg^IBr + products$ *Y* = Br, OH, NO_2, HO_2	k_{photo} [HgBrY]	*Saiz-Lopez et al.* [2018]

(a) All concentrations in brackets are in molecule cm^{-3}; [M] is the number density of air

We performed a number of test model runs for the period 2007-2013 using anthropogenic emissions for 2010 [*AMAP/UNEP*, 2013]. The first 6 years of the period were used for the model spin up to achieve the steady-state Hg concentrations in the troposphere. The model results are presented as annual averages for 2013. The list of the test model simulations is given in Table 2. Run #1 corresponds to model simulation with the Br oxidation chemistry and no Hg^{II} reduction. This simulation scenario has been already studied in detail and described in [*Ilyin et al.*, 2018]. Since products of Hg^{II} photo-dissociation are unknown we considered two different chemical scenarios of the photolysis reaction. The first scenario (Run #2) includes photo-reduction of Hg^{II} species

directly to Hg^0, whereas the second scenario (Run #3) considers monohalide HgBr as the main product of the reaction (see *Saiz-Lopez et al.* [2018] for the chemical explanation). Results of the model simulations were evaluated against a collection of ground-based measurements from at various regional and global monitoring networks described in [*Travnikov et al.*, 2017].

Table 2. *Model test runs for different atmospheric* Hg^{II} *reduction scenarios in the GLEMOS model*

Run ID	Scenario
Run #1	No Hg^{II} reduction (reactions *R*1-4)
Run #2	Gas phase Hg^{II} photo-reduction to Hg^0 (reactions *R*1-4, *R*5)
Run #3	Gas phase Hg^{II} photo-reduction to $Hg^{I}Br$ (reactions *R*1-4, *R*6)

Figure 6 shows global distributions of Hg^0 surface concentration simulated in different test runs as well as ground-based measurements at various monitoring sites. As seen all three spatial patterns reflect the inter-hemispheric gradient of Hg^0 concentration and similar areas of elevated concentrations related to major emissions regions (South and East Asia, Europe, North America, Equatorial Africa and South America). As it was mentioned in [*Ilyin et al.*, 2018] the model simulation with no Hg^{II} reduction (Run #1) leads to significant underestimation of measured Hg^0 concentrations, particularly, in remote regions of the Southern Hemisphere, where the effect of the atmospheric chemistry is the most pronounced (Fig. 6a).

Application of the photo-reduction mechanism with direct production of Hg^0 (Run #2) leads to insufficient net oxidation of Hg^0 in the atmosphere. It results in very long residence time and overestimated steady-state Hg^0 air concentrations in comparison with observations (Fig. 6b). In contrast, the other version of the mechanism with photo-reduction to HgBr (Run #3) provides more realistic levels and spatial distribution of Hg^0 concentration on a global scale (Fig. 6b).

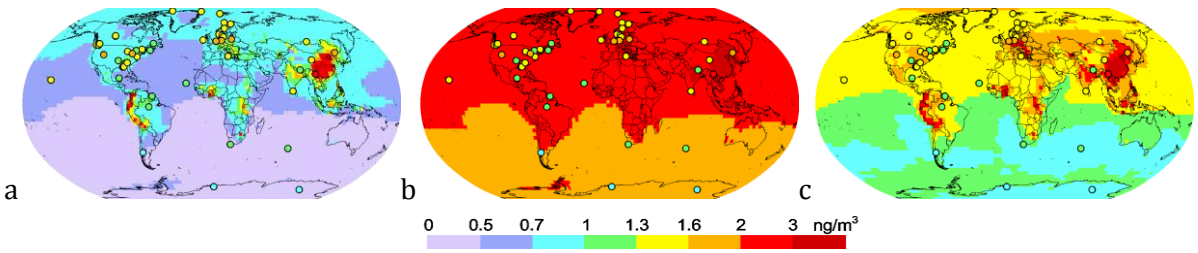

Fig. 6. *Spatial distribution of* Hg^0 *surface concentration for different tests: (a) – Run #1; (b) – Run #2; (c) – Run #3. Circles show observed values in the same color scale. The measurement dataset is the same as in Travnikov et al. [2017].*

More detailed evaluation of the modelling results against observations is shown in Fig. 7. The model Run #1 underestimates the observed Hg^0 air concentrations by 40% on average (Fig. 7a). It is accompanied by slight overestimation of measured Hg wet deposition (Fig. 7b). It indicates unrealistically strong oxidation capacity of the

atmosphere. Run #2 demonstrates twofold overestimation of Hg^0 measurements and almost 80% underestimation of observed wet deposition. In its turn, it implies the lack of Hg^0 oxidation in the atmosphere. Run #3 provides relatively good agreement of modelling results with measurements still containing 20% overestimation of Hg^0 air concentration and 20% underestimation of Hg wet deposition.

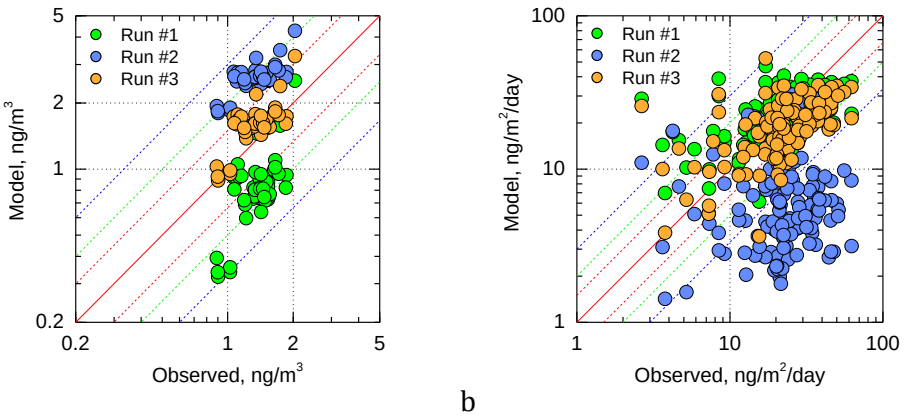

a b

Fig. 7. *Comparison of simulated* Hg^0 *air concentration (a) and* Hg *wet deposition (b) with measurements in 2013. The measurement dataset is the same as in Travnikov et al. [2017]*

More understanding of the oxidation and reduction processes can be obtained from analysis of the Hg chemical budget in the atmosphere (Fig. 8). Model estimates of the global atmospheric reservoir of Hg^0 are 1600, 7400 and 3800 Mg for the test Runs #1, #2 and #3, respectively. Only the last value is comparable with the previous estimates of 4000 Mg for the total atmosphere [e.g. *Travnikov et al.*, 2009; *Holmes et al.*, 2010] and 3500 Mg for the troposphere [*Horowitz et al.*, 2017].

The gas-phase oxidation by atomic Br leads to transformation of Hg^0 to a unstable intermediate HgBr, which decomposes back to Hg^0 or reacts further with various atmospheric compounds (e.g. Br, OH, HO_2, NO_2) to form Hg^{II} (Fig. 8a). Oxidized Hg^{II} species can photo-dissociate back to Hg^0 or to HgBr. Direct photolysis of Hg^{II} to Hg^0 shifts the redox equilibrium to the reduction direction leading to very high steady-state level of Hg^0 and low levels of Hg^{II} (Fig. 8b). In contrast, the photo-reduction pathway through photolysis of Hg^{II} to HgBr is limited by the following decomposition of HgBr to Hg^0. It results in slower rates of overall Hg^{II} reduction and higher atmospheric levels of the Hg^{II} species (Fig. 8c). The simulated Hg^{II} species in this model test (Run #3, Fig. 8c) are dominated by $HgBr_2$, which contributes 77% of total atmospheric Hg^{II}. The second largest Hg^{II} species is HgBrONO (15%), which is followed by HgBrOH (8%). Contribution of HgBrOOH is negligible.

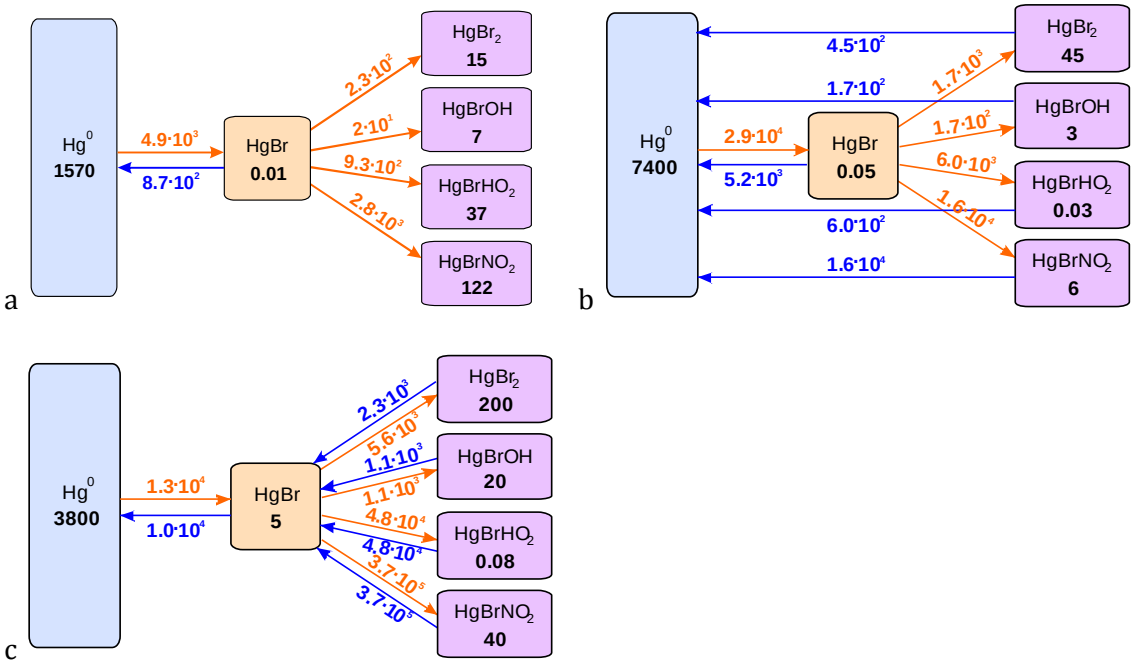

Fig. 8. *Global budget of Hg chemical cycling in the atmosphere for different tests: (a) – Run #1; (b) – Run #2; (c) – Run #3. The mass estimates are in* Mg *of* Hg*, the fluxes are in* Mg *of* Hg *per year*

The process of formation of the Hg^{II} species in the most realistic Run #3 is illustrated in Fig. 9. The figure shows distribution of average mixing ratios of $HgBr_2$, HgBrOH, HgBrOOH, and HgBOrNO in the atmosphere along with net production rates (production minus decomposition) of these species in appropriate reactions (R4 and R7, Table 1). The production rates depend on local concentrations of monohalide HgBr, concentration of appropriate oxidants (Br, OH, HO_2, NO_2), and air temperature. The decomposition rates are determined by the photolysis rate, which is a function of solar radiation, and concentration of Hg^{II} species. The dominant Hg^{II} species $HgBr_2$ is largely produced in the upper troposphere at high and temperate latitudes of both hemispheres and next to the surface at high latitudes of the Southern Hemisphere (Fig. 9a). Due to absence of removal factors Hg^{II} produced in the upper troposphere has long residence time that leads to its accumulation and high concentrations aloft. The lower atmosphere, particularly, of the tropical zone is characterized by net decomposition and lower concentrations of $HgBr_2$.

The second important Hg^{II} species, HgBrONO, is also mostly produced in the upper troposphere at high latitudes of the Southern and, in particular, Northern Hemispheres (Fig. 9d). These regions are also characterized by relatively high concentrations of the species in the free troposphere. HgBrOH has a maximum of the production rate in the upper troposphere of the tropics, where elevated concentrations of these species occur (Fig. 9b). The production and decomposition of HgBrOOH mostly compensate each other resulting in very low net production rates throughout the whole atmosphere with some shift to production in the upper atmosphere and to decomposition in the lower atmosphere. Therefore, the steady-state concentrations of this Hg^{II} species is very low

(Fig. 9c). All Hg^{II} species are depleted in the low troposphere of the Intertropical Convergence Zone due to intensive scavenging by precipitation.

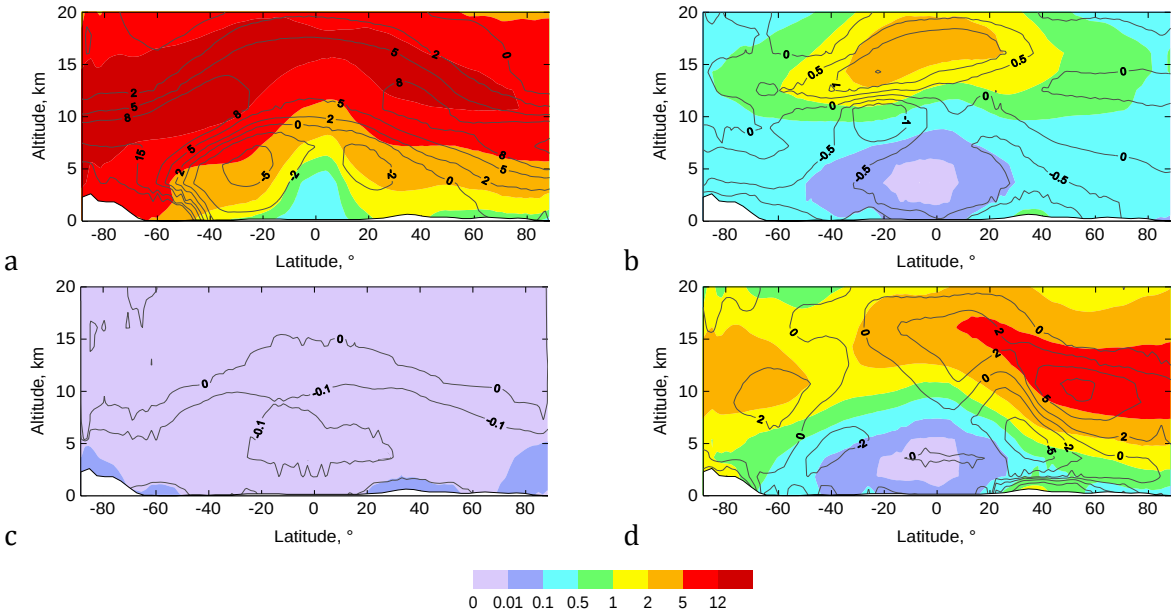

Fig. 9 *Annual zonal mean volume mixing ratios (colour palette,* ppqv Hg*) of* $HgBr_2$ *(a),* HgBrOH *(b),* $HgBrHO_2$ *(c),* HgBrONO *(d) for test Run #4. Isolines show net production rates (*10^2 *molecules* cm^{-3} s^{-1}*) for appropriate* Hg *species according to reactions R4 and R6 from Table 1. Positive values correspond to net production of* Hg^{II}*, negative values show net dissociation to* HgBr*.*

The photo-reduction mechanism significantly affects Hg global deposition pattern. Comparison of spatial distribution of Hg deposition simulated with no reduction (Run #1) and with the considered gaseous-phase photolysis (Run #3) is shown in Fig. 10. The photo-reduction mechanism decrease air concentrations of Hg^{II} and increase concentrations of Hg^0. It leads to decrease of dry and wet deposition of HgII all over the globe. In contrast, it increases dry deposition of Hg0, mostly, due to interaction with vegetation. Thus, effect of the photo-reduction consists of decreased Hg deposition over the ocean and increased deposition terrestrial vegetated areas. An exception is Hg deposition over the Southern ocean, where intensive Hg^0 oxidation largely prevails over Hg^{II} reduction and general increase of Hg^0 concentration leads to increased Hg deposition.

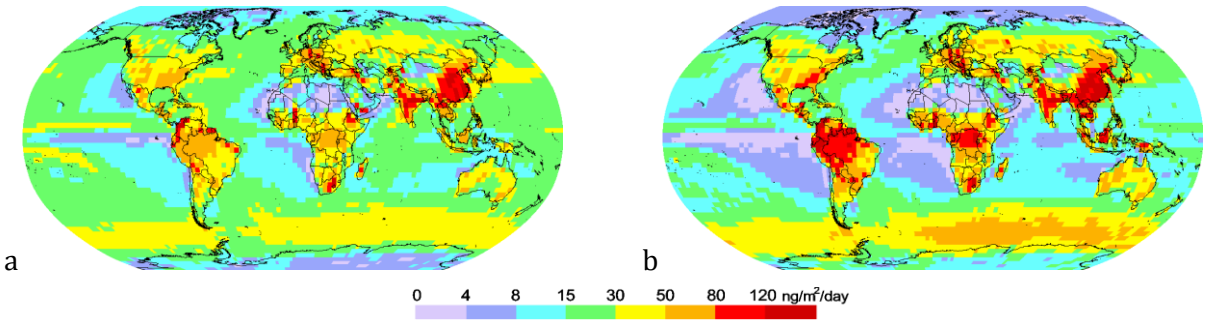

Fig. 10. *Spatial distribution of* Hg *total deposition for different tests: (a) – Run #1; (b) – Run #2; (c) – Run #3*

Thus, the analysis shows that the new gaseous photo-reduction mechanism applied along with the Br-initiated oxidation chemistry provides reasonable agreement of modelling results with observations. However, remaining discrepancies of modelling results with measurements require further in-depth study of the Br oxidation/reduction chemistry.

AMAP/UNEP [2013] Technical Background Report for the Global Mercury Assessment 2013a. Arctic Monitoring and Assessment Programme, Oslo, Norway / UNEP Chemicals Branch, Geneva, Switzerland, vi + 263 pp., available at: http://www.amap.no/documents/download/1265 (last access: 10 April 2018).

Amos H.M., Jacob D.J., Holmes C.D., Fisher J.A., Wang Q., Yantosca R.M., Corbitt E.S., Galarneau E., Rutter A.P., Gustin M.S., Steffen A., Schauer J.J., Graydon J.A., Louis V.L. St., Talbot R.W., Edgerton E.S., Zhang Y., and Sunderland E.M. [2012] Gas-particle partitioning of atmospheric Hg(II) and its effect on global mercury deposition, *Atmos. Chem. Phys.*, **12**, 591–603, doi:10.5194/acp-12-591-2012.

Balabanov N., Shepler B., Peterson K. [2005] Accurate global potential energy surface and reaction dynamics for the ground state of HgBr2*, J. Phys. Chem.* A, **109**, 8765—8773.

Dibble T.S., M.J. Zelie and H. Mao [2012] Thermodynamics of reactions of ClHg and BrHg radicals with atmospherically abundant free radicals. *Atmospheric Chemistry and Physics*, **12**:10271-10279.

Donohoue D., Bauer D., Cossairt B., and Hynes A. [2006] Temperature and pressure dependent rate coefficients for the reaction of Hg with Br and the reaction of Br with Br: A pulsed laser photolysispulsed laser induced fluorescence study, *J. Phys. Chem.* A, **110**, 6623–6632, doi:10.1021/jp054688j.

Emmons L.K., Walters S., Hess P.G., Lamarque J.-F., Pfister G.G., Fillmore D., Granier C., Guenther A., Kinnison D., Laepple T., Orlando J., Tie X., Tyndall G., Wiedinmyer C., Baughcum S.L., and Kloster S. [2010] Description and evaluation of the Model for Ozone and Related chemical Tracers, version 4 (MOZART-4), *Geosci. Model Dev.*, **3**, 43–67, doi:10.5194/gmd-3-43-2010.

Goodsite M.E., Plane J.M.C. and Skov H. [2004] A Theoretical Study of the Oxidation of Hg0 to HgBr2 in the Troposphere, *Environ. Sci. Technol.*, **38**, 1772–1776.

Holmes C.D., Jacob D.J., Corbitt E.S., Mao J., Yang X., Talbot R., and Slemr F. [2010] Global atmospheric model for mercury including oxidation by bromine atoms, *Atmos. Chem. Phys.*, **10**, 12037–12057, doi:10.5194/acp-10-12037-2010.

Horowitz H.M., D.J. Jacob, Y. Zhang, T.S. Dibble, F. Slemr, H.M. Amos, J.A. Schmidt, E.S. Corbitt, E.A. Marais and E.M. Sunderland [2017] A new mechanism for atmospheric mercury redox chemistry: Implications for the global mercury budget. *Atmospheric Chemistry and Physics Discussions*, **1-33**, 10.5194/acp-2016-1165.

Ilyin I., O.Rozovskaya, O.Travnikov, W. Aas, K.A. Pfaffhuber [2018] Assessment of heavy metal transboundary pollution on global, regional and national scales. EMEP Status Report 2/2018.

Jiao Y. and Dibble T.S. [2017] First kinetic study of the atmospherically important reactions BrHg + NO2 and BrHg + HOO, *Phys. Chem. Chem. Phys.*, **19**, 1826–1838, doi:10.1039/c6cp06276h.

Parrella J.P., Jacob D.J., Liang Q., Zhang Y., Mickley L.J., Miller B., Evans M.J., Yang X., Pyle J.A., Theys N., and Van Roozendael M. [2012] Tropospheric bromine chemistry: implications for present and pre-industrial ozone and mercury, *Atmos. Chem. Phys.*, **12**, 6723–6740, doi:10.5194/acp-12-6723-2012.

Saiz-Lopez A., Sitkiewicz S.P., Roca-Sanjua¡n D., Oliva-Enrich J.M. , Da¡valos J.Z. , Notario R., Jiskra M., Xu Y., Wang F., Thackray C.P., Sunderland E.M., Jacob D.J., Travnikov O., Cuevas C.A., Acuana A.U., Rivero D., Plane J.M.C., Kinnison D.E., Sonke J.E. [2018] Photoreduction of gaseous oxidized mercury changes global atmospheric mercury speciation, transport and deposition. *Nature Comm.* **9**, 4796, doi: 10.1038/s41467-018-07075-3.

Travnikov O., Angot H., Artaxo P., Bencardino M., Bieser J., D'Amore F., Dastoor A., De Simone F., Diéguez M.D.C., Dommergue A., Ebinghaus R., Feng X.B., Gencarelli C.N., Hedgecock I.M., Magand O., Martin L., Matthias V., Mashyanov N., Pirrone N., Ramachandran R., Read K.A., Ryjkov A., Selin N.E., Sena F., Song S., Sprovieri F., Wip D., Wängberg I., and Yang X. [2017] Multi-model study of mercury dispersion in the atmosphere: atmospheric processes and model evaluation, *Atmos. Chem. Phys.*, **17**, 5271-5295, doi:10.5194/acp-17-5271-2017.

Travnikov O., Jonson J.E., Andersen A.S., Gauss M., Gusev A., Rozovskaya O., Simpson D., Sokovyh V., Valiyaveetil S., and Wind P. [2009] Development of the EMEP global modelling framework: Progress report. EMEP/MSC-E Technical Report 7/2009, Meteorological Synthesizing Centre – East of EMEP, Moscow, 44 pp., available at: http://www.msceast.org/index.php/publications/reports (last access: 19 June 2018).